J Biomol NMR (2015) 61:173–180
DOI 10.1007/s10858-015-9901-3

NMR STRUCTURE NOTE

The RING domain of human promyelocytic leukemia protein (PML)

Shu-Yu Huang · Chi-Fon Chang · Pei-Ju Fang · Mandar T. Naik · Peter Güntert · Hsiu-Ming Shih · Tai-huang Huang

Received: 6 December 2014 / Accepted: 19 January 2015 / Published online: 28 January 2015

Biological context

The post-translational modification of attaching ubiquitin (Ub) or ubiquitin-like proteins (UbL) to proteins is an important mechanism in regulating many cellular processes (Pickart 2001). These modifications resulted in diverse effects, ranging from modulation of protein structure, functions, or localization to protostome-dependent proteolysis. The modification process is achieved through a cascade involving several enzymes, the E1 activating enzyme, the E2 conjugating enzyme, and the E3 ligating enzyme. Interaction of the E3 ligases with E2 and substrate proteins confers substrate specificity and promotes transfer of Ub or UbL from E2 enzymes to the substrates. There are two major types of ubiquitin E3 ligases in eukaryotes, defined by the presence of either a homologous to the E6AP carboxyl terminal (HECT) or a really interesting new gene (RING) domain. The HECT domains serve as catalytic intermediates in ubiquitination whilst the RING domains confer specificity to ubiquitin by binding to E2-ubiquitin thioester and activate transfer of ubiquitin to substrates. RING E3 ligases are zinc-finger containing domains conserved from yeast to humans (Deshaies and Joazeiro 2009; Freemont et al. 1991). There are over 600 RING-based ubiquitin E3 genes potentially expressed in human cells, constituting the largest family of proteins. Thus, RING E3 ligases have been linked to numerous cellular processes and human diseases (Deshaies and Joazeiro 2009).

PML is a member of the tripartite motif-containing protein (TRIM/RBCC) that form a superfamily with ~70 members in humans and mice (Meroni 2012). All PML isoforms harbors the conserved N-terminal tripartite motif

Electronic supplementary material The online version of this article (doi:10.1007/s10858-015-9901-3) contains supplementary material, which is available to authorized users.

S.-Y. Huang · P.-J. Fang · M. T. Naik · H.-M. Shih · T. Huang (✉)
Institute of Biomedical Sciences, Academia Sinica, Nankang, Taipei 11529, Taiwan, ROC
e-mail: bmthh@ibms.sinica.edu.tw

S.-Y. Huang
Chemical Biology and Molecular Biophysics Program, Taiwan International Graduate Program, Institute of Biological Chemistry, Academia Sinica, Nankang, Taipei 11529, Taiwan, ROC

S.-Y. Huang
Institute of Biochemical Sciences, College of Life Science, National Taiwan University, Taipei 10617, Taiwan, ROC

C.-F. Chang · T. Huang
Genomics Research Center, Academia Sinica, Nankang, Taipei 11529, Taiwan, ROC

M. T. Naik
Department of Biochemistry and Biophysics, Texas A&M University, 300 Olsen Boulevard, College Station, TX 77843-2128, USA

P. Güntert
Institute of Biophysical Chemistry, Center for Biomolecular Magnetic Resonance, Frankfurt Institute of Advanced Studies, 60438 Frankfurt am Main, Germany

T. Huang
Department of Physics, National Taiwan Normal University, Taipei 11677, Taiwan, ROC

(TRIM/RBCC) containing three cysteine-rich zinc-binding domains, a RING domain, two B-boxes (B-box 1 and B-box 2) and a coiled-coil region but differ either in the central region or in the C-terminal region (Bernardi and Pandolfi 2007; Jensen et al. 2001). PML is the major component and the key organizer of the PML nuclear bodies (PML NBs) that contain many critical regulators and mediate significant activities, such as transcriptional regulation, antiviral defense, DNA replication, DNA repair, telomere lengthening, chromatin organization, cell cycle control, senescence, apoptosis, and tumor suppression (Carracedo et al. 2011; Bernardi and Pandolfi 2007). PML NBs are highly SUMOylated and their functions are strongly associated with SUMOylation process (Lallemand-Breitenbach et al. 2001). PML contains three SUMOylation sites (K65, K160 and K490) and directly interacts with Ubc9 (Duprez et al. 1999). Using the tumor suppressor p53 and its principal antagonist Mdm2 as substrates Chu et al. found that PML associated with Ubc9, p53 and Mdm2 and functions as a E3 ligase (Chu and Yang 2011). The E3 activity of PML depends on intact structures of the RING motif and B-box domains. However, detailed structural information of the interactions is not known. We have solved the structure of PML B-box 1 (Huang et al. 2014) and the structure of the PML RING domain has been solved previously by ^{1}H homonuclear NMR (Borden et al. 1995). Here we report the solution structure of PML RING, solved by heteronuclear multi-dimensional NMR. Surprisingly, our structure is significantly different from that reported previously. The goodness of these two structures are compared and the potential sources of discrepancy are discussed.

Methods and results

Cloning, expression, and purification of recombinant proteins

The PML RING domain (residues 49–104) was PCR amplified with flanking BamHI and XhoI restriction sites (Fig. 1a, b). The PCR products were then cloned into pGEX4T-1 that contained an N-terminal GST tag followed by thrombin cleavage site. All constructs were transformed into BL21(DE3) and selected by ampicillin (*Sigma*). Clones were cultured in M9 minimal medium supplemented with 20 μm $ZnCl_2$ and incubated at 37 °C until $OD_{600} \sim 0.8$. Induction condition was at 18 °C at the 0.2 mM IPTG as the final concentration. Overnight induced cells were harvested and lysed in buffer 50 mM Tris, 300 mM NaCl, 10 mM BME, 0.1 mM $ZnCl_2$, pH7.5. By using glutathione Sepharose 4B (*GE Healthcare*), expressed GST fusion proteins were purified and further passed through size-exclusion column (*GE Superdex 75 16/60*) in 25 mM Tris (pH7.0), 100 mM NaCl, 1 mM $ZnCl_2$ and 0.2 mM Tris (2-carboxyethyl) phosphine (TCEP) (*Sigma*).

NMR spectroscopy and resonance assignments

NMR experiments were conducted at 25 °C using a Bruker Avance 600 MHz NMR spectrometer equipped with 5 mm triple resonance cryoprobe and single axis pulsed field gradient. Sequence specific assignments of backbone resonances were made from analysis of HNCA, HNCO, CBCA(CO)NH, and HNCACB spectra. Side chain resonances were assigned from the combined information content of the ^{15}N-edited TOCSY-HSQC, HCCH-TOCSY, H(CC)(CO)NH, (H)CC(CO)NH, (HB)CB(CGCD)HD, and (HB)CB(CGCDCE)HE spectra. ^{1}H chemical shifts were externally referenced to 0 ppm methyl resonance of 2,2-dimthyl-2-silapentane-5-sulfonate (DSS), whereas ^{13}C and ^{15}N chemical shifts were indirectly referenced according to the IUPAC recommendations (Markley et al. 1998). NMR data were processed using the software Topspin 2.0 and analyzed by the software SPARKY (T. D. Goddard and D. G. Kneller, SPARKY 3, University of California, San Francisco, CS, USA). 95.1 % of the ^{1}H, ^{15}N and ^{13}C resonances of the PML RING domain have been assigned (Fig. 1c) and the assignment data have been deposited in the BioMagResBank under accession numbers 25376.

NOE distance restraints were obtained from ^{15}N-edited NOESY-HSQC and ^{13}C-edited NOESY-HSQC spectra obtained with PML RING domain at 1.0 mM concentration. The backbone dihedral angle restraints for Φ and Ψ were empirically predicted by the TALOS software program (Cornilescu et al. 1999). Hydrogen bonds derived from CSI prediction (Wishart and Sykes 1994) were introduced as pairs of distance restraints. The structures were first calculated with Cyana v3.9 program (Guntert 2009) without zinc until the structures were well converged. At this stage the zinc ions were added using the coordination reported in the PML RING domain structure (PDB ID: 1BOR) (Borden et al. 1995). Introduction of the zinc ions did not produce additional NOE violation. The validities of the cysteine residues assigned to coordinate to zinc ion were further confirmed from the calculated probabilities from $^{13}C^{\alpha}$, $^{13}C^{\beta}$ and secondary structure assignments as suggested by Kornhaber et al. (2006). The results are all greater than 0.5 (C57, 0.96; C60, 0.98; C72, 0.81; C77, 0.85; C80, 0.93; C88, 0.81; C91, 0.99). The tautomeric state of His74 was also assessed from the chemical shift of $C^{\delta 2}$ (126.6 ppm) and $C^{\varepsilon 1}$ (138.1 ppm) (Sudmeier et al. 2003). The results suggest that His74 exist as the $N^{\delta 1}$–H tautomer with the zinc ion coordinated to $N^{\varepsilon 2}$. This is in agreement with our structural calculation that showed that

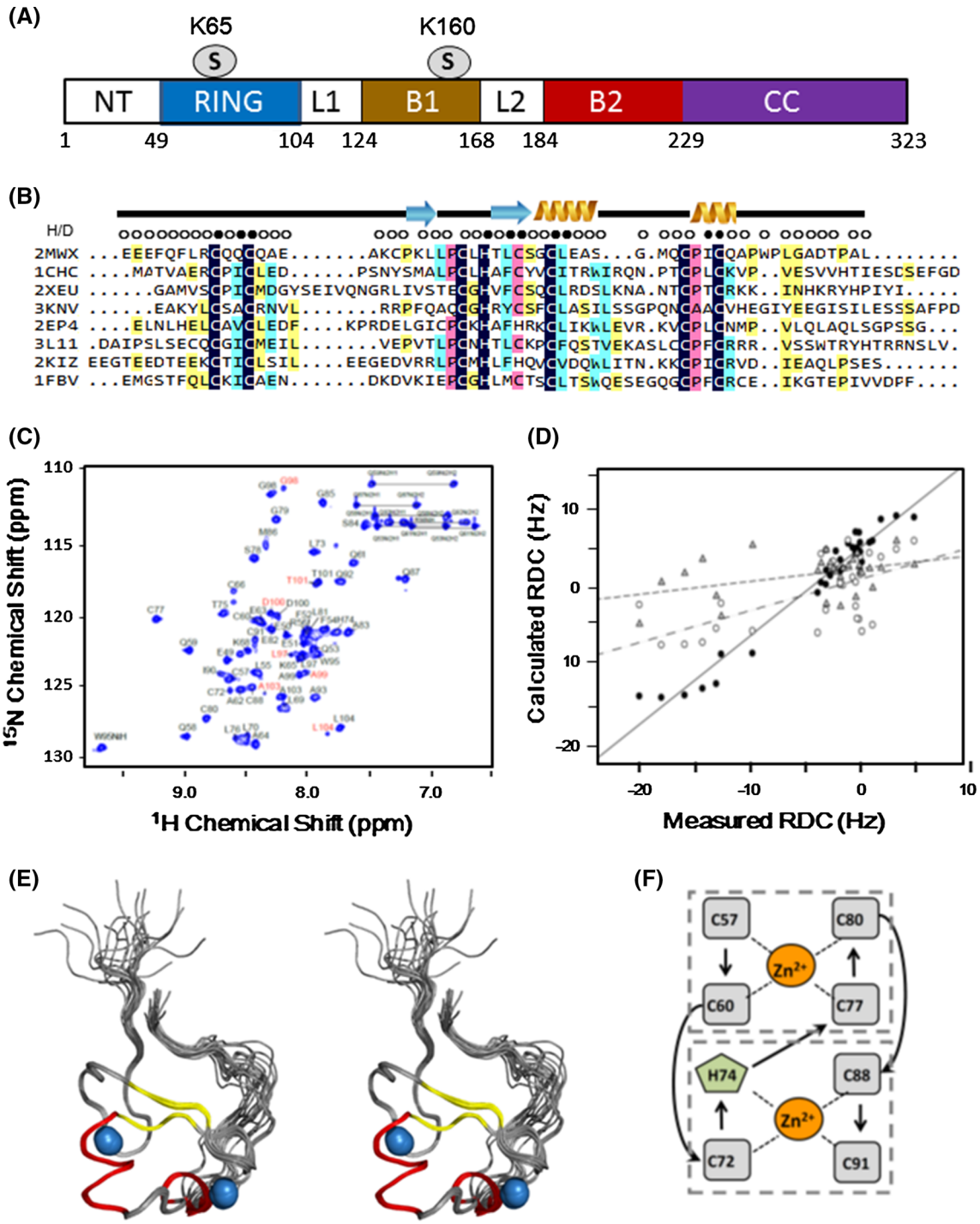

Fig. 1 **a** Structural organization of the TRIM motif of promyelocytic leukemia protein (PML). **b** Sequence alignment of the PML RING domain with other RING domains, identified with their PDB codes (1MWX, PML RING; 1CHC, C3HC4 zinc finger domain; 2XEU, RNF4; 3KNV, TRAF2 RING domain; 2EP4, RNF24; 3L11, RNF168; 2KIZ, Arkadia RING-H2 domain; 1FBV, c-Cbl RING domain). *Color codes* represent degrees of homologies: *Black*, 100 %; *pink*, 75 %; *cyan*, 50 %; *pink*, 35 %. The secondary structures of PML RING domain are shown on top of the sequence 3. *Blue arrows* represent β strands and the *coils* represent α helices. The H/D exchange rates are shown below the secondary structure bar. The *filled circles* are residues with slow H/D exchange rates and the *open circles* are residues with fast H/D exchange. **c** ^{15}N-HSQC of PML RING domain (a.a. 49–104). Resonance assignments are labeled. The residues showing two peaks are labeled *red*. **d** Correlation between measured and predicted residual backbone ^{1}H-^{15}N dipolar couplings before (*open circles*) and after (*filled circles*) structure refinement with RDC. The *open triangles* are predicted RDC for PML RING structure reported previously (PDB ID: 1BOR) (Borden et al. 1995). **e** Stereo view of the overlay of 20 PML RING structures. The α-helix segments are colored *red* and the β-strand segments are colored *yellow*. The *blue* spheres are the zinc ions. **f** Schematic of the cross-braced zinc coordination of PML RING domain

the $N^{\delta 1}$–H tautomer gave much better results. The quality of the restraints was checked by analyzing the violations of the calculated conformers using the MolMol (Koradi et al. 1996) and Procheck (Laskowski et al. 1996) software programs. The structure of PML RING domain has been deposited in the Protein Data Bank with PDB ID: 2MWX.

The ^{15}N-R_1, ^{15}N-R_2, and [^{1}H–^{15}N]-NOE were determined by using standard pulse sequences. Each ^{15}N-R_1 was determined with delays of 0, 90, 190, 310, 460, 650, 930, and 1,500 ms. Similarly, each ^{15}N-R_2 was determined from delays of 0, 17, 34, 68, 119, 170, 237, and 339 ms. Both rate constants were determined using the program Protein Dynamics Center (Bruker, Germany), assuming a mono-exponential decay of the peak intensities. The errors in peak intensities were calculated from two duplicate experiments. The steady-state heteronuclear [^{1}H–^{15}N] NOE experiment was carried out in duplicate in an interleaved manner, with and without proton saturation. The NOE was calculated as the error-weighted average ratio of peak intensities, with errors estimated by the standard deviation of three pairs of repeated experiments. The reduced spectral density analysis was performed as previously described (Lefevre et al. 1996).

Overview of the PML RING structure

The NMR resonances of PML RING domain (a.a. 49–104) were assigned both manually to 95.1 % completeness and further cross-check with auto-assignment by FLYA program in Cyana3.9 (Fig. 1c) (Schmidt and Guntert 2012). The secondary structure predicted from chemical shift indices showed that the PML RING domain consists of two β strands and two α helices arranged in the following topology: ββαα (β1, a.a. 67–69; β2, a.a. 75–77; α1: a.a. α1, 78–84; α2: a.a. 89–92) (supplemental Figure S1). The solution structure of the PML RING domain was computed based on 685 NOE distance restrains (364 short, 105 medium and 216 long), 14 hydrogen bond restraints, and 68 dihedral-angle restrains. The structures were further refined with 31 ^{15}N–^{1}H residual dipolar coupling restraints with a final correlation of predicted and measured RDC of 97.9 % (Fig. 1d). The overlay of the backbone traces of 20 best structures is shown on Fig. 1e. A summary of structure statistics for the 20 best structures (Table 1) showed a pairwise root mean square deviation (RMSD) of 0.26 Å for the backbone atoms and 0.62 Å for the heavy atoms for the structured region comprising residues Leu55–Ala93. PROCHECK (Laskowski et al. 1996) analysis showed that 79.3 % of residues are in the most favored region, 20.0 % in the additionally allowed region, and 0.7 % in the generously allowed region and 0 % in the disallowed regions.

The dominant feature of the PML RING structure is the presence of two zinc fingers folded in the "cross-brace" mode (Fig. 1f). Zinc ions are absolutely required as addition of EDTA resulted in a complete collapse to an unstructured state as characterized by the congregation of all H^N resonances to the 7.8–8.7 ppm region in the proton dimension (Data not shown). The N terminal segment from Glu49 to Phe54 and the C-terminal segment from Pro94 to Ile104 are disordered. The first zinc finger is a C4-type with the zinc atom coordinated to Cys57, Cys60, Cys77 and Cys80. The second zinc finger is a C3H1-type with the zinc atom coordinated to Cys72, His74, Cys88 and Cys91 in a tetrahedral geometry. The two β strands form an anti-parallel hairpin and α2 is a short 3_{10}–helix. Interestingly, we observed two sets of resonances with relative population ratio of 0.7:0.3 for the C-terminal residues from Leu97–Leu104, suggesting the existence of two conformations for this region. The segment is preceded by a Pro94–Trp95–Pro96 sequence. Structure calculation and NOE patterns showed that Pro94 exists in the trans-form whilst the second Pro96 can be in either trans- or cis-conformation. The C-terminal segment folds back, and could potential interact with the β hairpin region.

Table 1 NMR structure calculation and refinement statistics for PML RING domain

NMR distance and dihedral constraints	RING
Distance constraints	
Total NOE	685
Short range ($\|i-j\| \leq 1$)	364
Medium-range ($1 < \|i-j\| < 5$)	105
Long-range ($\|i-j\| \geq 5$)	216
Hydrogen bonds	14
Total dihedral angle restraints	
ϕ	
Ψ	34
Residual dipolar couplings restraints (RDC)	31
Average pairwise r.m.s. deviation[a] (Å)	
Backbone	0.26 ± 0.08
Heavy atom	0.62 ± 0.10
Ramachandran plot[b]	
Residues in most favorable regions (%)	79.3 %
Residues in additional favorable regions (%)	20.0 %
Residues in generously favorable regions (%)	0.7 %
Residues in disallowed regions (%)	0.0 %

[a] The RMSD was calculated for residues 55–93

[b] The Ramachandran plot was generated by PROCHECK for the 20 energy minimization structures for residues 55–93

Dynamics of the PML RING domain

To gain further structural insights, we investigated the backbone dynamics of PML RING by reduced spectral density functions calculated from amide ^{15}N-R1, ^{15}N-R2

and [^{1}H–^{15}N]-NOE at 600 MHz (Fig. 2). Overall, the PML RING domain is rigid for the structured region between residues Phe55–Ala93 with an average R1 value of 2.49 s^{-1}, R2 of 7.16 s^{-1} and an average ^{1}H–^{15}N NOE of 0.7. The rotational correlation time of PML RING domain estimated from the R2/R1 ratios of residues in the rigid part of the molecule is 2.88 ns, consistent with the predicted value of a monomeric protein of similar size. As expected, the terminal residues are highly flexible with NOEs dropping below 0. Nonetheless, PML RING showed several distinctive dynamic features: (1) The loop region proceeding the β1 strand and including residues Cys66 and the SUMOylation site Lys65 showed significant disorder as indicated by the substantial drop in NOE values to 0.4 and higher J(ω_N) value, indicative of the presence of nano-micro second dynamics. The motional flexibility for this region likely plays a role in PML SUMOylation by either promoting the recognition with SUMO E2 conjugating enzyme, Ubc9, and/or facilitating SUMO transfer from Ubc9. (2) Residues Met86 and Cys91 exhibit much higher J(0) values, suggesting the presence of msec slow motion. Residue Met86 is located in the middle of the hinge region between the two zinc fingers, indicating that the probable presence of breathing fluctuations between the two domains. (3) Residues Leu97 and Gly98 have larger J(ω_N) values, indicative of the presence of nano-μsec motion for

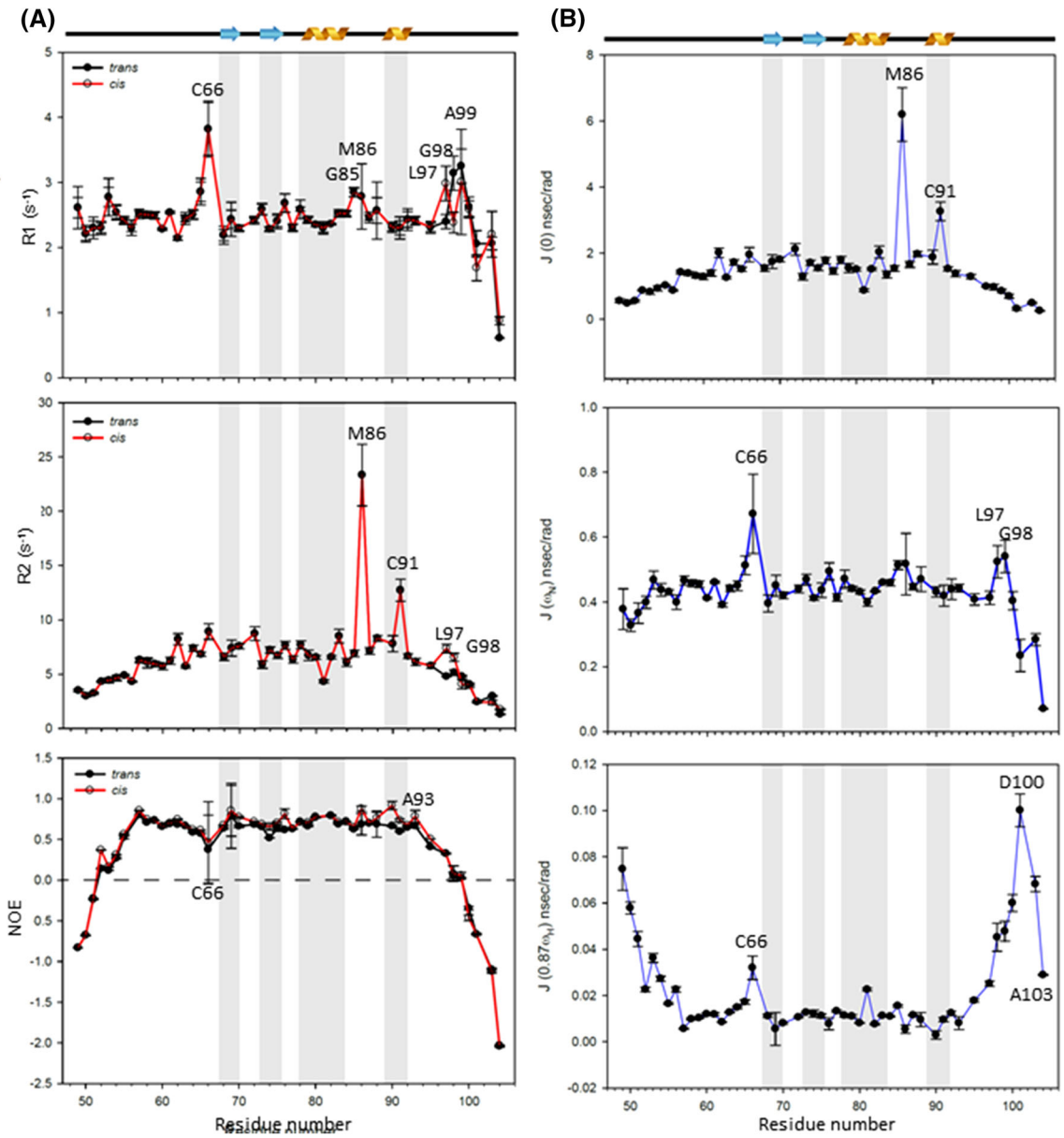

Fig. 2 Dynamics of PML RING domain. **a** ^{15}N-R1 (*top*), ^{15}N-R2 (*middle*) and [^{1}H-^{15}N]-NOE data of trans- (*black*) and cis-form (*red*) of PML RING domain. **b** Reduced spectral density functions (trans-form) deduced from relaxation data shown in (**a**)

the C-terminal loop. Interestingly, the C-terminal residues Thr101–Ala103 showed a significant decrease in $J(\omega_N)$ and $J(*0.87\omega_H)$ suggesting that the C-terminal tail of PML RING may be partially constrained.

Discussion and conclusion

The solution structure of PML RING domain has been solved previously by ^{1}H homonuclear NMR methods (PDB ID: 1BOR) (Fig. 1d) (Borden et al. 1995). As shown on Fig. 3a, b, the 1BOR structure is very different from ours solved by heteronuclear NMR (PDB ID: 2MWX) with a RMSD of 9.262 Å. Comparison of the secondary structures revealed that the two inner β strands, i.e. β2′ and β3′, in the 1BOR structure correspond to the β1 and β2 strands in the 2MWX structure whilst the two terminal β strands, i.e. β1′ and β4′, were not observed in the 2MWX structure (Fig. 3c). The two structures are most similar in the core region composing the β1 and β2 strands. The absence of β1′ and β4′ was supported by the observation of very small ^{1}H–^{15}N–NOE for residues 53–56 and negative values for residues 101–104, indicating that the β1′ and β4′ segments are highly flexible. Significantly, the two helices reported in the 1BOR structure were both shifted four residues down the sequence observed in the 2MWX structure. We then compared our structure with several RING domain structures reported in the literature (Fig. 3d). The RMSDs of the structured region (a.a. Leu55–Ala93) between 2MWX structure and other RING domains are: 1.184 Å for RNF4 (magenta, PDB ID: 2XEU), 1.395 Å for TRAF2 (pink, PDB ID: 3KNV); 2.824 Å for RNF24, (blue, PDB ID: 2EP4); 1.297 Å for RNF168 (cyan, PDB ID: 3L11); 2.384 Å for H2E3 ligase (grey, PDB ID 2KIZ); and 3.353 Å for C-cbl RING (orange, PDB ID 1FBV). We concluded that the folding of the core RING domain of all these proteins are highly homologous to our 2MWX structure. To further examine the goodness of 2MWX and 1BOR structures we measured the residual dipolar coupling constants (RDC) and compare them with those calculated from the two structures (Fig. 1d). The RDCs calculated from the 2MWX structure fit much better than those calculated from the 1BOR structure even before refinement. We further measured the hydrogen/deuterium (H/D) exchange rates of H^Ns of all residues (Fig. 1b). The results showed that the most protected residues are located in the two zinc finger regions. Significantly, several slow exchange H^Ns are within the two helices regions assigned in the 2MWX structure, but none in the helices regions assigned by 1BOR. Thus, the H/D exchange results also support the secondary structure assignments of 2MWX, but not 1BOR. However, the source of the structure discrepancy

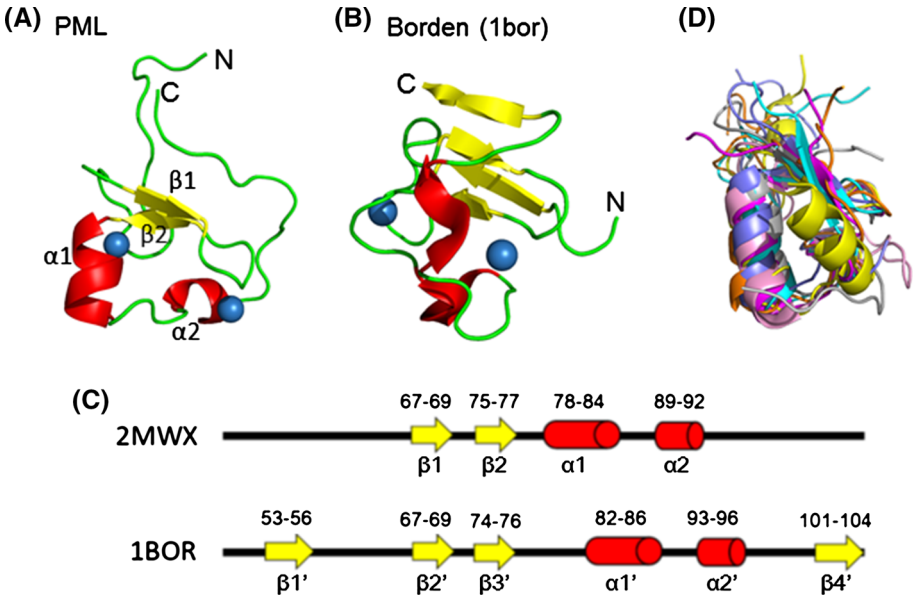

Fig. 3 Comparison of the RING structures. **a** PML RING domain structure reported in this paper (PDB ID, 2MWX). **b** PML RING domain structure determined by Borden et al. (PDB ID, 1BOR) (1995). The β1 and βs strands were used to align the two structures. Color codes for (**a**) and (**b**): *blue*, zinc ions; *red*, helices; *yellow*, β strands; *green*, loops. **c** Alignment of the secondary structures of PML RING domain reported in the present study (2MWX) and that reported by Borden et al. (1BOR) (1995). **d** Overlay of the structures of PML RING (*red*, PDB ID: 2MWX), TRAF2 Zinc finger (*blue*, PDB ID: 3KNV), RNF4 (*magenta*, PDB ID: 2XEU), RNF168 (*yellow*, PDB ID: 3L11); RNF24 (*blue*, PDB ID: 2EP4); equine herpes virus IE110 protein (IEEHV) (*cyan*, PDB ID: 1CHC): c-Cbl RING (*orange*, PDB ID, 1FBV); and Arkadia RING-H2 domain (*grey*, PDB ID 2KIZ)

could not be cross-checked since the NMR data employed for the structure calculation of 1BOR were not deposited in BMRB. We notice that the 1BOR and 2MWX structures were determined under similar buffer and pH conditions but the sample for determining 1BOR structure was a synthetic peptide refolded in the presence of Zn^{+2} whereas our protein was expressed and purified directly from *E. coli* grown in the presence of 20 μM Zn^{+2}. We further noticed that the number of NOE restraints used in calculating the 1BOR structures is only half of those used in calculating the 2MWX structure (42 medium range and 93 long range NOEs as compared to 105 medium and 216 long range NOEs in 2MWX structure).

Recently, Chu and Yang showed that TRIM proteins bind both the SUMO conjugating enzyme Ubc9 and SUMO substrates to enhance transfer of SUMOs from Ubc9 to these substrates (Chu and Yang 2011). The SUMO E3 activity appears to be prevalent among TRIM proteins and they proposed that TRIM proteins are a new class of SUMO E3 s. The activity of TRIM proteins requires intact RING and B-box domains. RING domains are recognized as the major class of ubiquitin E3 ligases (Deshaies and Joazeiro 2009; Metzger et al. 2014). Thus, a single TRIM protein can have dual E3 activities. A continuum may exist among TRIM proteins in the relative strength of the ubiquitin and SUMO E3 activity; some TRIM proteins may modulate their target protein primarily through ubiquitination while others through SUMOylation. A TRIM protein may also attach ubiquitin and SUMO onto the same target simultaneously or sequentially to achieve versatile outcomes. PML contains three SUMOylation sites at Lys65 in the RING domain, Lys160 in B-box 1 and Lys490 in the C-terminal region. SUMOylation of Lys160 by SUMO2/3 can lead to poly-SUMOylation which can be recognized by the poly-SIMs domain of RNF4, a SUMO targeted ubiquitin ligase (STUbL), leading to degradation of PML (Tatham et al. 2008). Thus, it is important to dissect the molecular basis of the PML TRIM motif as ubiquitin or SUMO E3 ligase. We have previously solved the structure of the PML B-box 1 domain (Huang et al. 2014). The determination of a high resolution structure of the PML RING domain reported here is essential for further understanding of the molecular basis of E2–E3-substrate recognition of SUMOylation and ubiquitination of the PML system.

Acknowledgments The NMR experiments were conducted on NMR spectrometers at the High-Field Nuclear Magnetic Resonance Center (HFNMRC), supported by the National Research Program for Biopharmaceuticals, the National Science Council of the Republic of China. We acknowledge the use of Biophysics Core Facility at Academia Sinica, Taiwan. This work was supported by grants from the Ministry of Science and Technology, Republic of China, to T.H.H. (NSC101-2311-B-001-025; NSC102-2113-M-001-010).

References

Bernardi R, Pandolfi PP (2007) Structure, dynamics and functions of promyelocytic leukaemia nuclear bodies. Nat Rev Mol Cell Biol 8:1006–1016

Borden KL, Boddy MN, Lally J, O'Reilly NJ, Martin S, Howe K, Solomon E, Freemont PS (1995) The solution structure of the RING finger domain from the acute promyelocytic leukaemia proto-oncoprotein PML. EMBO J 14:1532–1541

Carracedo A, Ito K, Pandolfi PP (2011) The nuclear bodies inside out: PML conquers the cytoplasm. Curr Opin Cell Biol 23:360–366

Chu Y, Yang X (2011) SUMO E3 ligase activity of TRIM proteins. Oncogene 30:1108–1116

Cornilescu G, Delaglio F, Bax A (1999) Protein backbone angle restraints from searching a database for chemical shift and sequence homology. J Biomol NMR 13:289–302

Deshaies RJ, Joazeiro CA (2009) RING domain E3 ubiquitin ligases. Annu Rev Biochem 78:399–434

Duprez E, Saurin AJ, Desterro JM, Lallemand-Breitenbach V, Howe K, Boddy MN, Solomon E, de The H, Hay RT, Freemont PS (1999) SUMO-1 modification of the acute promyelocytic leukaemia protein PML: implications for nuclear localisation. J Cell Sci 112(Pt 3):381–393

Freemont PS, Hanson IM, Trowsdale J (1991) A novel cysteine-rich sequence motif. Cell 64:483–484

Guntert P (2009) Automated structure determination from NMR spectra. Eur Biophys J Biophys Lett 38:129–143

Huang SY, Naik MT, Chang CF, Fang PJ, Wang YH, Shih HM, Huang TH (2014) NMR structure note: the B-box 1 dimer of human promyelocytic leukemia protein. J Biomol NMR 60:275–281

Jensen K, Shiels C, Freemont PS (2001) PML protein isoforms and the RBCC/TRIM motif. Oncog Res 20:7223–7233

Koradi R, Billeter M, Wüthrich K (1996) MOLMOL: a program for display and analysis of macromolecular structures. J Mol Gr 14:51–55

Kornhaber G, Snyder D, Moseley HB, Montelione G (2006) Identification of zinc-ligated cysteine residues based on 13Cα and 13Cβ chemical shift data. J Biomol NMR 34:259–269

Kung CC, Naik MT, Wang SH, Shih HM, Chang CC, Lin LY, Chen CL, Ma C, Chang CF, Huang TH (2014) Structural analysis of poly-SUMO chain recognition by RNF4-SIMs domain. Biochem J 462:53–65

Lallemand-Breitenbach V, Zhu J, Puvion F, Koken M, Honore N, Doubeikovsky E, Duprez E, Pandol PP, Puvion E, Freemont PS, de The H (2001) Role of promyelocytic leukemia (pml) sumolation in nuclear body formation, 11 s proteasome recruitment, and As2o3-induced PML or PML/retinoic acid receptor α degradation. J Exp Med 193:1361–1371

Laskowski RA, Rullmann JAC, MacArthur MW, Kaptein R, Thornton JM (1996) AQUA and PROCHECK-NMR: programs for checking the quality of protein structures solved by NMR. J Biomol NMR 8:477–486

Lefevre JF, Dayie KT, Peng JW, Wagner G (1996) Internal mobility in the partially folded DNA binding and dimerization domains of GAL4: NMR analysis of the N-H spectral density functions. Biochemistry 35:2674–2686

Markley JL, Bax A, Arata Y, Hilbers CW, Kaptein R, Sykes BD, Wright PE, Wuthrich K (1998) Recommendations for the presentation of NMR structures of proteins and nucleic acids. IUPAC-IUBMB-IUPAB inter-union task group on the standardization of data bases of protein and nucleic acid structures determined by NMR spectroscopy. J Biomol NMR 12:1–23

Meroni G (2012) Genomics and evolution of the TRIM gene family. Adv Exp Med Biol 770:1–9

Metzger MB, Pruneda JN, Klevit RE, Weissman AM (2014) RING-type E3 ligases: master manipulators of E2 ubiquitin-conjugating enzymes and ubiquitination. Biochim Et Biophys Acta Mol Cell Res 1843:47–60

Pickart CM (2001) Mechanisms underlying ubiquitination. Annu Rev Biochem 70:503–533

Schmidt E, Guntert P (2012) A New algorithm for reliable and general NMR resonance assignment. J Am Chem Soc 134: 12817–12829

Sudmeier JL, Bradshaw EM, Haddad KEC, Day RM, Thalhauser CJ, Bullock PA, Bachovchin WW (2003) Identification of histidine tautomers in proteins by 2D 1H/13Cδ2 one-bond correlated NMR. J Am Chem Soc 125:8430–8431

Tatham MH, Geoffroy MC, Shen L, Plechanovova A, Hattersley N, Jaffray EG, Palvimo JJ, Hay RT (2008) RNF4 is a poly-SUMO-specific E3 ubiquitin ligase required for arsenic-induced PML degradation. Nat Cell Biol 10:538–546

Wishart DS, Sykes BD (1994) Chemical shifts as a tool for structure determination. Methods Enzymol 239:363–392